

Lignin's ability to nucleate ice via immersion freezing and its stability towards physicochemical treatments and atmospheric processing

Sophie Bogler¹, Nadine Borduas-Dedekind^{1,2}

5 ¹Institute for Biogeochemistry and Pollutant Dynamics, ETH Zurich, Zurich, 8092, Switzerland

²Institute for Atmospheric and Climate Sciences, ETH Zurich, Zurich, 8092, Switzerland

Correspondence to: nadine.borduas@usys.ethz.ch, @nadineborduas

10 Table of Contents

Section S1. Ion chromatography calibration curves.....	2
Section S2. Freezing of background water filtered with PTFE and Cellulose acetate filters	2
Section S3. Method details: photochemistry and actinometry	3
Section S4. Details FINC - Ice Nucleation Setup	5
15 Section S5. TOC analysis.....	7
Section S6. Effect of sonication on lignin's IN activity: Freezing temperature boxplot	8
Section S7. Effect of H ₂ O ₂ on lignin's IN activity: Freezing temperature boxplot, freezing temperature boxplots for control 4 day experiment and UV/Vis absorption spectra.....	8
Sect S9. Effects of atmospheric processing on lignin's chemical structure: UV/Vis absorption spectra and IC results	12

Section S1. Ion chromatography calibration curves

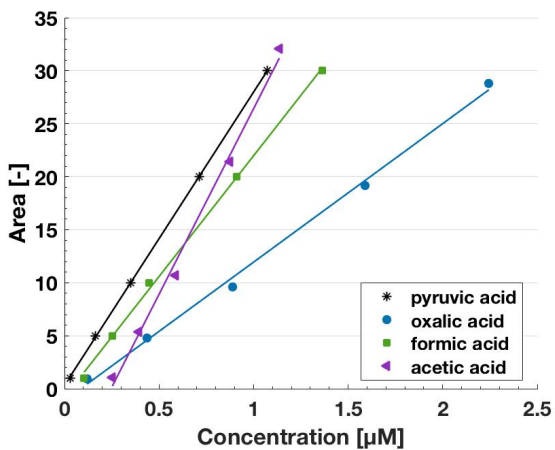


Figure S1: IC calibration curves. Linear fit $R^2 > 0.99$ for all four analysed small low-molecular weight organic acids.

Section S2. Freezing of background water filtered with PTFE and Cellulose acetate filters

30

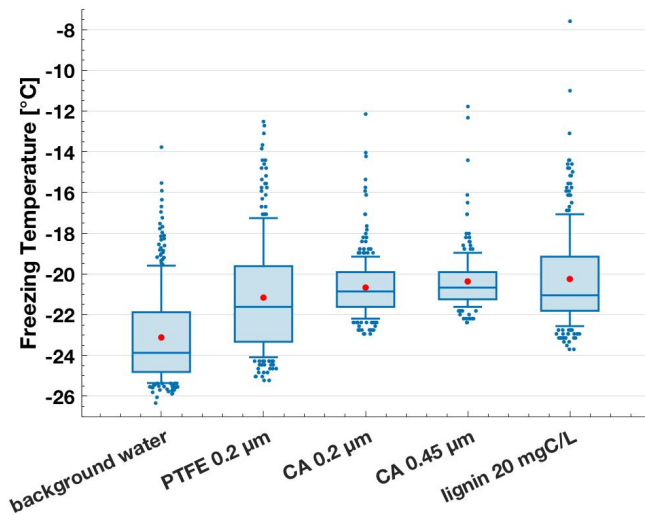


Figure S2: Freezing temperatures determined by FINC with background water after filtration with PTFE membrane (BGB®, USA) and Cellulose acetate filters (VWR™, USA). The use of these filters for lignin size filtration was not continued as their background IN activity equals lignin's IN activity at 20 mg C L^{-1} possibly due to abraded IN active filter material or insufficient rinsing before use.

35 Section S3. Method details: photochemistry and actinometry

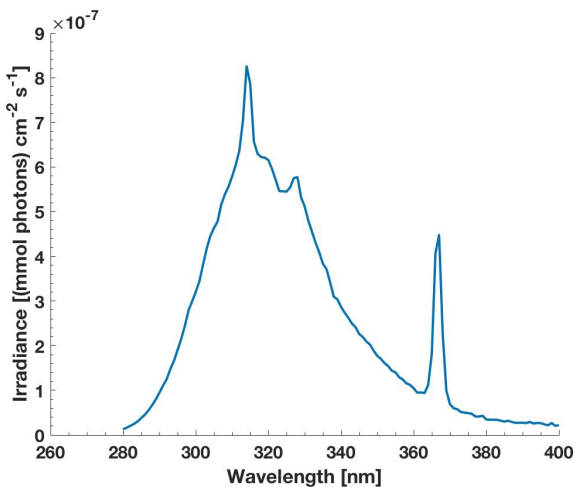
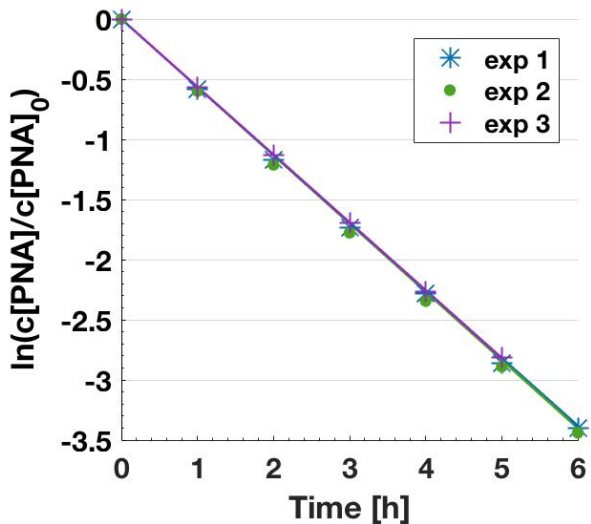


Figure S3: Spectral irradiance as a function of wavelength of photochemical setup using 8×300 nm UVB light bulbs, measured by a portable UV/Vis spectrophotometer (Ocean Optics) and calibrated with actinometry experiment.



40 Figure S4: Logarithmic plot of concentration decay with time of actinometer PNA quantified via HPLC. Linear regression fit was calculated for each experiment 1-3, $R^2 > 0.99$ for each fit. The slope of each fit provides one pseudo first-order degradation constant $k_{\text{deg,PNA}}$. The average value of all three experiments with one standard deviation was $k_{\text{deg,PNA}} = -0.568 \pm 0.004 \text{ h}^{-1}$.

3.1 Calculation of absolute spectral irradiance

The light intensity of the photochemical setup using 8×300 nm light bulbs was used to calculate the absolute spectral irradiance $I_\lambda = s \times I_{\lambda,m}$. I_λ is scaled (factor s) from the known spectral irradiance $I_{\lambda,m}$, which was previously measured in the photoreactor with a calibrated Jaz spectrophotometer (Ocean Optics) using 2×300 nm UVB bulbs and was corrected for the absorption of the borosilicate test tubes between 280-300 nm (Borduas-Dedekind et al., 2019). The scaling factor s is calculated with Eq. S1.

$$\text{Eq. S1: } s = \frac{k_{deg,PNA} * [PNA]_0 * l}{\phi_{deg,PNA} * \sum_\lambda (I_{\lambda,m} * f_{\lambda,PNA}) \Delta \lambda}$$

In Eq.S1, $[PNA]_0 = (23.5 \pm 0.18)$ μM is the average PNA concentration at timepoint 0 h from 3 experiments and $l = 1.14$ cm is the light pathlength of the borosilicate test tube. $\Phi_{deg,PNA} = 3.63 \times 10^{-4}$ is the direct photolysis quantum yield which was calculated following Laszakovits et al., 2016. $f_{\lambda,PNA}$ is the fraction of light absorbed by the PNA starting solution and was calculated with Eq.S2, where $\epsilon_{\lambda,PNA}$ is the molar extinction coefficient of PNA. $I_{\lambda,m}$ and $f_{\lambda,PNA}$ are summed up from 280 nm to 400 nm in steps of $\Delta\lambda = 1$ nm.

$$\text{Eq. S2: } f_{\lambda,PNA} = 1 - 10^{-\epsilon_{\lambda,PNA} * [PNA]_0 * l}$$

With a scaling factor of $s = 375.89$, this calculation resulted in an absolute spectral irradiance $I_\lambda = (109.94 \pm 0.85)$ W m^{-2} .

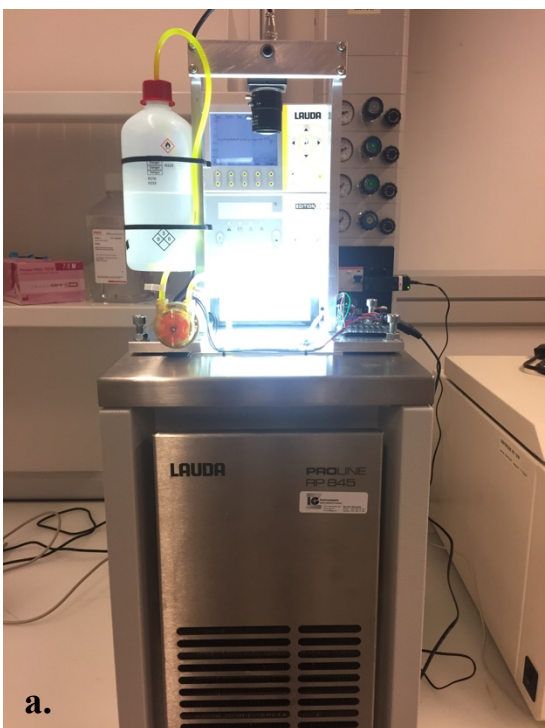
3.2 Calculation of equivalent sunlight conditions

To compare the experimental conditions to environmental sunlight conditions, a conversion factor c_{sun} from the irradiation time in the photoreactor into the equivalent irradiation time in natural sunlight is introduced. c_{sun} is the ratio of the rate of light absorption in lignin solution samples irradiated by I_λ ($R_{\text{abs}}^{\text{photoreactor}}$, Eq.S3) over the equivalent rate by irradiation with $I_{\lambda,\text{sun}}$ ($R_{\text{abs}}^{\text{sun}}$), the simulated solar irradiance (Apell and McNeill, 2019).

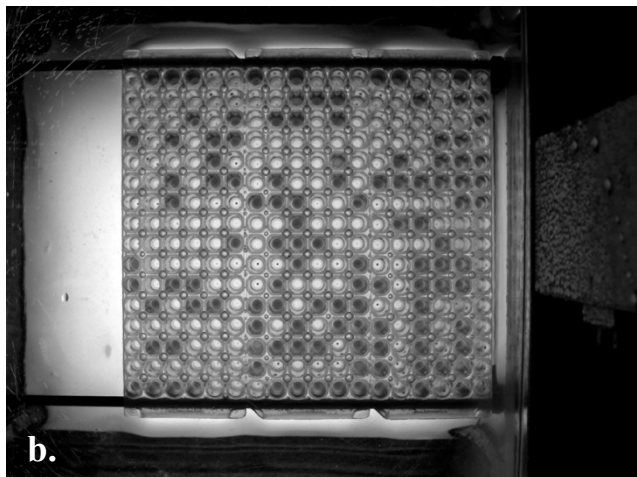
$$\text{Eq. S3: } R_{\text{abs}}^{\text{photoreactor}} = \frac{1}{l} \sum_\lambda I_\lambda (1 - 10^{-A_{\lambda,\text{lignin}}})$$

In Eq. S3, $A_{\lambda,\text{lignin}}$ is the absorbance of a 20 mg C L^{-1} lignin solution at 0 h of UVB irradiation. For $R_{\text{abs}}^{\text{sun}}$, I_λ in Eq. S3 is replaced by $I_{\lambda,\text{sun}}$, which was simulated as in Borduas-Dedekind et al., 2019, giving an integrated irradiance of 59.2 J $\text{s}^{-1} \text{m}^{-2}$ between 280 nm and 400 nm. Using the resulting conversion rate of $c_{\text{sun}} = 3.14$, 25 h in the photoreactor equipped with 8 UVB light bulbs equals an irradiation of 78.6 h sunlight, or 6.5 days in the environment. This conversion assumes 12 h of sunlight for a clear day.

Section S4. Details FINC - Ice Nucleation Setup



a.



b.

75

Figure S5: Ice Nucleation Setup a.) FINC instrument b.) Picture of piko PCR trays taken by the FINC camera during an ongoing sample run showing the change in contrast between liquid (light) and frozen state (dark) of each well.

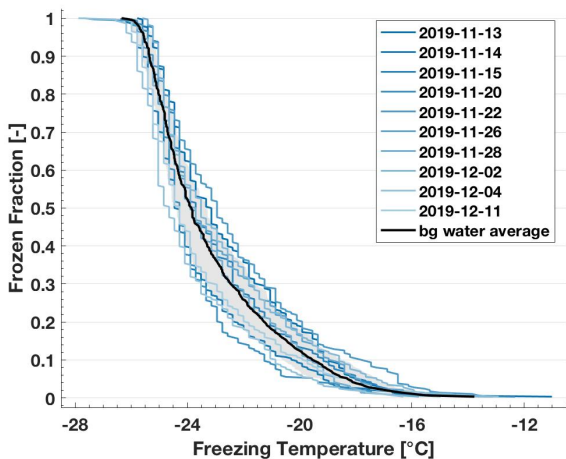
4.1 FINC data processing

80 FINC's raw data are the pictures taken during cooling and the corresponding recorded Lauda bath temperature. These images are processed with automated picture analysis in MATLAB®, first developed by David et al. (2019). First, each well location is detected and then a freezing event is assigned to each well at the time the greatest change in light intensity occurred between two pictures (details in Miller et al., 2020). A vector containing the freezing temperatures of all 288 wells is the main output. These freezing temperatures are finally calibrated with a temperature calibration (Eq. S4) to account for the difference between
85 the Lauda recorded bath temperature (T_{bath}) and the temperature within each well (T_{well}). The temperature calibration was conducted with a 12-channel thermo-couple logger (Lutron Electronic, BTM-4208SD) before starting the freezing experiments for this study and validated again after the freezing experiments were completed (Miller et al., 2020). The reported freezing temperatures in the manuscript are all calibrated with Eq. S4 and shown as T_{well} .

90 Eq. S4: $T_{\text{well}} = 0.75 + 0.95 * T_{\text{bath}}$

95 **4.2 FINC limit of detection determination**

The background of FINC was determined by averaging 10 consolidated freezing curves of Sigma Aldrich molecular biology water (background water), used as a pure background water standard (Figure S6). One standard deviation at each 1/288 step describes the uncertainty in FINC's limit of detection. On average, the lower temperature limit of FINC is at -23.9 ± 0.6 °C when 50% wells are frozen. Spontaneous homogeneous freezing of pure water with a rate < 1s would occur at -32 °C in a droplet of 20 µL. We explain the difference based on the water quality and contaminations introduced through the working environment. Note that the spontaneous homogenous freezing at temperatures as low as -38 °C as observed in the atmosphere requires small pico-L droplet volumes to fall below a rate of 1s.



105 **Figure S6: FINC background determination results based on averaged background water (bg water average). 10 freezing curves of bg water are shown in blue color as stepwise function, titled after date of measurement. One standard deviation of the average represents the uncertainty of the limit of detection and is shown in grey shading.**

4.3 Reproducibility within FINC of 20 mg C L⁻¹ lignin solutions

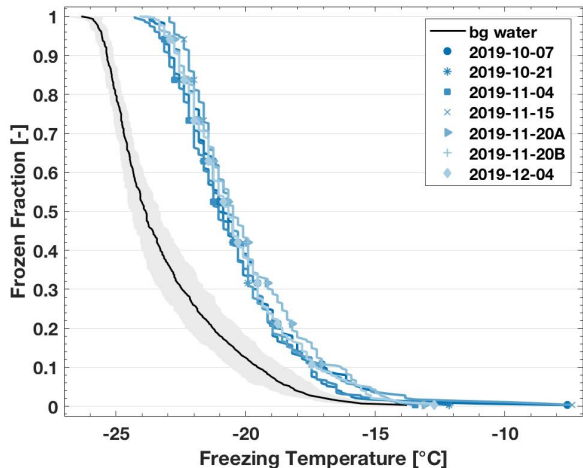


Figure S7: FF curves for seven FINC experiments with 20 mg C L⁻¹ untreated lignin solutions from the same bulk solution conducted over a 2-month period. The T₅₀ is -20.8 ± 0.2 °C showing the stability of the IN activity in the lignin bulk solution and the reproducibility within FINC experiments.

Section S5. TOC analysis

To record changes in the carbon content of lignin sample solutions after treatments and atmospheric processing, we attempted to quantify their total organic carbon content, specifically the non-purgeable organic carbon (NPOC). The measurement was done using a total organic carbon (TOC) analyser (Shimadzu, model TOC-L CSH). The instrument's method was set to 50 µL injections up to 4 times per sample, the sparge time was 90 sec and the sparge gas flow was 80 mL min⁻¹. The results were reported as concentrations in mg C L⁻¹ with standard deviation from the average based on a linear calibration curve from recrystallized potassium phthalate that ranged from 5 to 200 mg C L⁻¹ ($R^2 = 0.9997$).

In preliminary measurement runs with freshly prepared aqueous lignin solutions, we noticed that the instrument's platinum oxidation catalyst for the combustion process did not successfully combust lignin. The quantified NPOC values from the TOC analyzer was only ~ 60 % of the expected NPOC value of 20 mg C L⁻¹, based on the weighed solid lignin and on the manufacturer's carbon content analysis. For lignin solutions of 200 mg C L⁻¹, the TOC analysis reported values of 5 mg C L⁻¹ for all samples, indicating an even worse conversion. In another attempt, we pre-treated the lignin solutions with 0.5 mL of 35-w% of H₂O₂ as an oxidant to help decompose lignin and consequently help the TOC combustion process. However, this addition did not have an effect on the quantification.

We hypothesize that this TOC analyzer's setup was not apt to analyze lignin due to its robust and recalcitrant polymeric chemical structure and subsequent method optimization attempts were unsuccessful. Therefore, we were not able to track changes in the carbon content of the lignin solutions. Instead, we rely on the carbon content as specified from Sigma-Aldrich for this study and report the starting value in the lignin solutions before further treatments or atmospheric processing experiments.

Section S6. Effect of sonication on lignin's IN activity: Freezing temperature boxplot

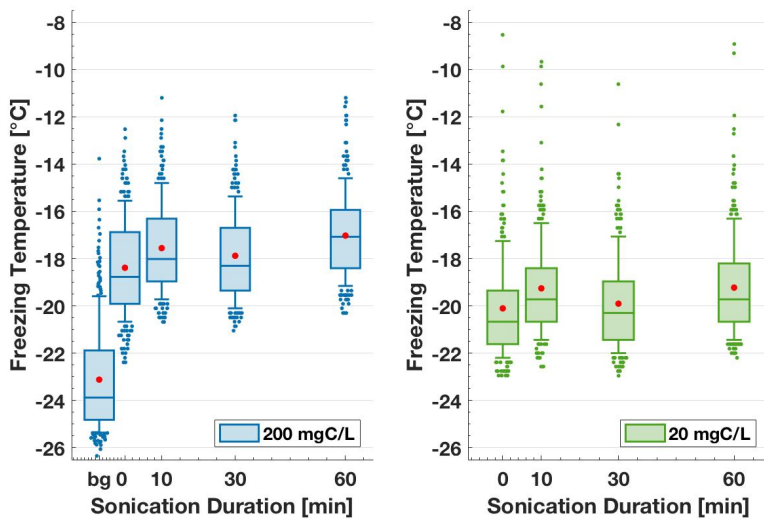


Figure S8: Freezing temperature boxplots after sonication of aqueous lignin solutions as physicochemical treatment. *Bg* refers to background water. Sonication did not introduce a distinct change on lignin's IN activity.

Section S7. Effect of H₂O₂ on lignin's IN activity: Freezing temperature boxplots and UV/Vis absorption spectra

In the reaction series of lignin with hydrogen peroxide no change in IN activity was observed up to the ratio 1 g lignin : 100 mL H₂O₂. At higher concentrations of hydrogen peroxide, an odd freezing point depression governed the decrease of the freezing temperatures down to the T₅₀ value of the hydrogen peroxide background at – 27.9 °C (Figure S9). This hydrogen peroxide background was prepared in the same manner as a lignin solution sample in the ratio 1 g lignin : 750 mL H₂O₂ but without adding any lignin. Notably, the determined T₅₀ value of this hydrogen peroxide background falls 4.1 °C below the background water's T₅₀ value. Increasing the hydrogen peroxide ratio in the background to 1 g lignin : 1000 mL H₂O₂ further enhanced the depression, so much so that the lower temperature limit in FINC was reached (– 36 °C) before complete freezing of all wells was observed. Similar incomplete freezing of the 288 wells was also observed in the 1 g lignin : 1000 mL H₂O₂ experiment.

The lower background of the hydrogen peroxide control complicates the interpretation of lignin's IN activity at ratios higher than 1 g lignin : 100 mL H₂O₂. It is difficult to deconvolute a possible freezing point depression with reaction with hydrogen peroxide. Indeed, lowering the lignin concentration would lower the IN activity (see Sect. 3.1.1), but tracking this possible decrease in concentration was unsuccessful.

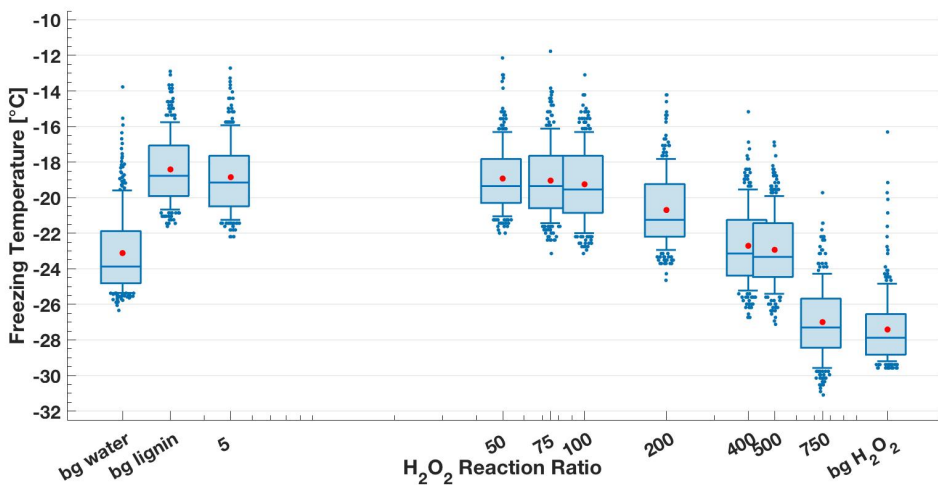


Figure S9: Freezing temperature boxplots for the reaction series with H₂O₂. The log x-axis displays the reaction ratio of 1 g lignin to x mL H₂O₂ (35-w%) before dilution with background water to 200 mg C L⁻¹. Bg lignin refers to a measurement of a 200 mg C L⁻¹ lignin solution without H₂O₂. Bg H₂O₂ is a background control prepared like a lignin sample in the ratio 1 g lignin : 750 mL H₂O₂ but without actual addition of lignin. Bg water refers to background water.

160

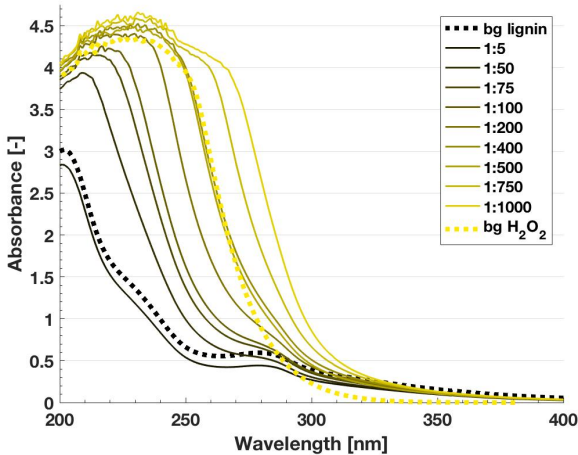


Figure S10: Absorption spectra for reaction series with H₂O₂ illustrating the increasingly overlaying signal of H₂O₂ over lignin. The reaction ratio is given in the legend as 1 g lignin : 5-1000 mL H₂O₂. The dashed lines of bg lignin and bg H₂O₂ refer to background measurements of only lignin concentrated 200 mg C L⁻¹ in background water and only H₂O₂ prepared like a lignin sample in the ratio 1 g lignin : 750 mL H₂O₂ but without addition of lignin.

165

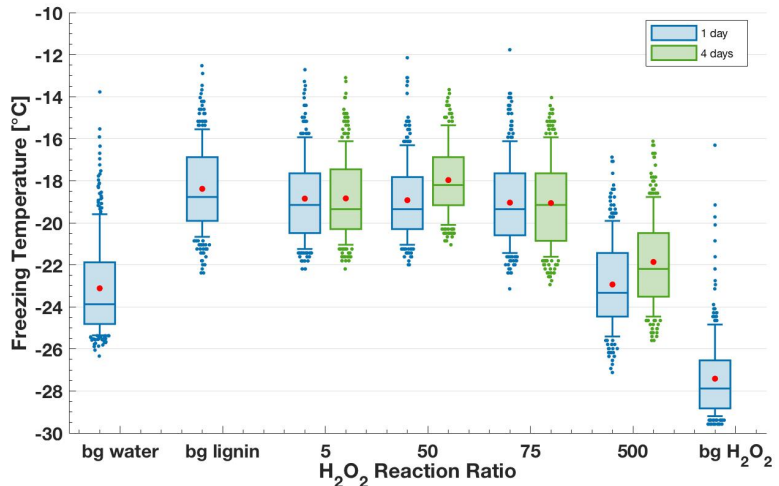


Figure S11: Freezing temperature boxplots for the control reaction series with H₂O₂ with prolonged reaction time to 4 days. The additional 3 days of reaction time did not introduce any change in the freezing temperatures. The log x-axis displays the reaction ratio of 1 g lignin to x mL of H₂O₂ (35-w%) before dilution with background water to 200 mg C L⁻¹. *Bg water* refers to background water. *Bg lignin* refers to a measurement of a 200 mg C L⁻¹ lignin solution without H₂O₂. *Bg H₂O₂* is a background control prepared like a lignin sample in the ratio 1 g lignin : 750 mL H₂O₂ but without actual addition of lignin.

Section S8. Effects of atmospheric processing on lignin's IN activity: Freezing temperature boxplots

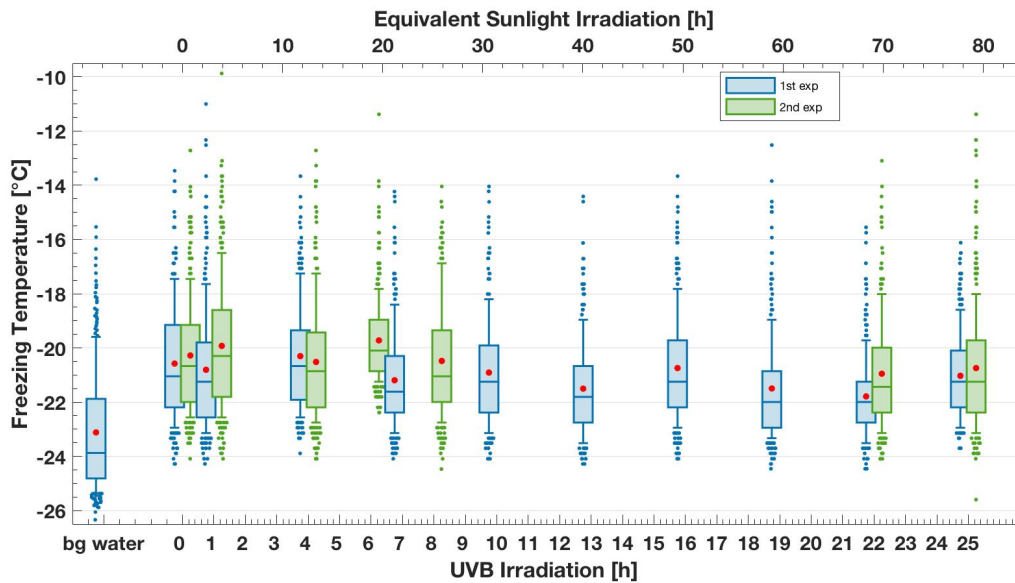


Figure S12: Freezing temperature boxplots of 20 mg C L^{-1} lignin solutions after exposure to UVB irradiation as atmospheric processing experiment. Includes two 25h-experiments which each equal 6.5 days in the environment. After 25 h UVB irradiation, the change in T_{50} value was less than $-1 \text{ }^{\circ}\text{C}$.

175

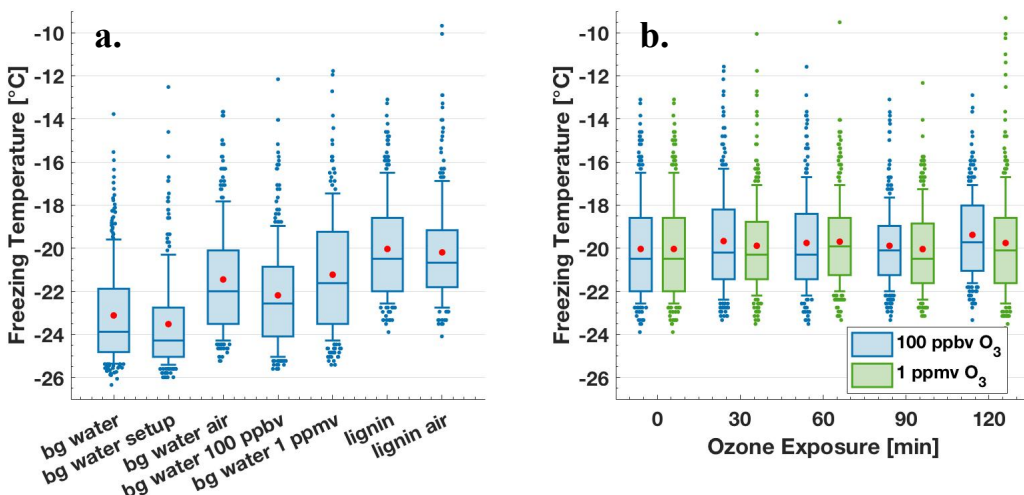


Figure S13: Freezing temperature boxplots of 20 mg C L^{-1} lignin solutions after exposure to ozone as atmospheric processing experiment. (a) Background control experiments were conducted to ensure stable background conditions: In *Bg water setup*, the bg water was collected after flushing through the glassware in the ozonation setup. *Bg water air* and *lignin air* refer to controls where filtered air was bubbled through the solutions for 30 min, but the ozone generator stayed turned off. (b) Freezing temperature boxplots for ozonation series with 20 mg C L^{-1} lignin bulk solution.

180

Sect S9. Effects of atmospheric processing on lignin's chemical structure: UV/Vis absorption spectra and IC results

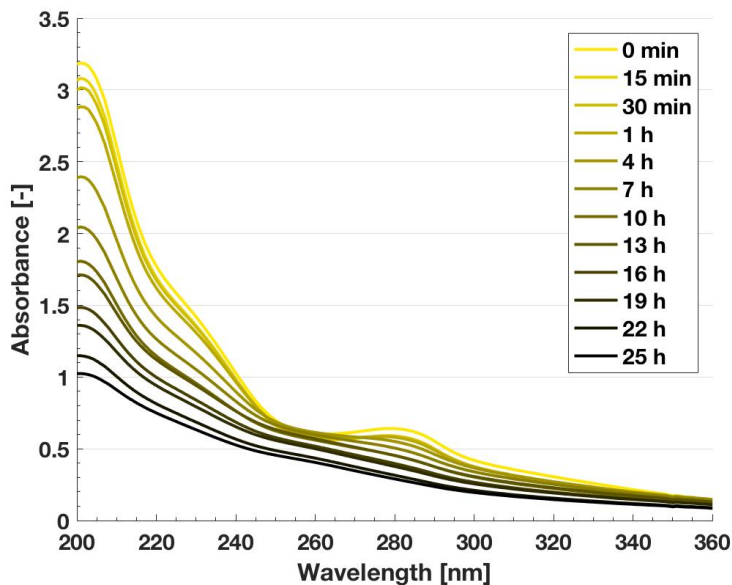


Figure S14: Absorption spectra for 20 mg C L^{-1} lignin solutions after atmospheric processing by UVB irradiation. With increasing exposure duration, lignin's absorbance is decreasing.

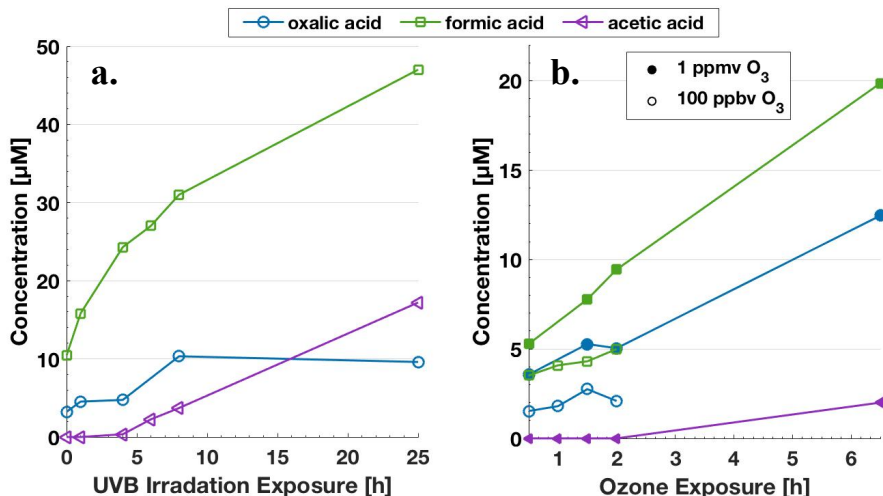


Figure S15: Formation of low molecular weight organic acids from lignin upon (a.) UVB irradiation and (b.) exposure to ozone (O_3). Pyruvic acid was below the detection limit in all samples, acetic acid was detected in all samples but the samples from exposure to 100 ppb O_3 . Note that in (b.) the timepoint 0 min was not measured and that the values for 1 h of 1 ppm O_3 exposure for oxalic acid and formic acid and for 6 h UVB irradiation for oxalic acid are missing due to a measurement error.

References

- 195 Apell, J. N. and McNeill, K.: Updated and validated solar irradiance reference spectra for estimating environmental photodegradation rates, *Environ. Sci.: Processes Impacts*, 21(3), 427–437, doi:10.1039/C8EM00478A, 2019.
- Borduas-Dedekind, N., Ossola, R., David, R. O., Boynton, L. S., Weichlinger, V., Kanji, Z. A. and McNeill, K.: Photomineralization mechanism changes the ability of dissolved organic matter to activate cloud droplets and to nucleate ice crystals, *Atmospheric Chemistry and Physics Discussions*, 1–27, doi:10.5194/acp-2019-427, 2019.
- 200 David, R. O., Cascajo-Castresana, M., Brennan, K. P., Rösch, M., Els, N., Werz, J., Weichlinger, V., Boynton, L. S., Bogler, S., Borduas-Dedekind, N., Marcolli, C. and Kanji, Z. A.: Development of the DRoplet Ice Nuclei Counter Zurich (DRINCZ): validation and application to field-collected snow samples, *Atmospheric Measurement Techniques*, 12(12), 6865–6888, doi:<https://doi.org/10.5194/amt-12-6865-2019>, 2019.
- 205 Laszakovits, J. R., Berg, S. M., Anderson, B. G., O'Brien, J. E., Wammer, K. H. and Sharpless, C. M.: p-Nitroanisole/pyridine and p-nitroacetophenone/pyridine actinometers revisited: Quantum yield in comparison to ferrioxalate, *Environmental Science & Technology Letters*, 4(1), 11–14, doi:<https://doi.org/10.1021/acs.estlett.6b00422>, 2016.
- Miller, A., Brennan, K., Mignani, C., Wieder, J., Zipori, A. and Borduas-Dedekind, N.: Development of a drop Freezing Ice Nuclei Counter (FINC) and using soluble lignin as an atmospheric ice nucleation standard, (manuscript in submission for Atmos. Meas. Tech. Disc.), 2020.

210